Infrared study of lattice and magnetic dynamics in a spin-chain compound Gd$_2$BaNiO$_5$

S. A. Klimin,[1] A. B. Kuzmenko,[2] M. N. Popova,[1] B. Z. Malkin,[3] and I. V. Telegina[4]

[1]*Institute of Spectroscopy, RAS, 142190 Troitsk, Moscow region, Russia*
[2]*DPMC, University of Geneva, 1211 Geneva 4, Switzerland*
[3]*Physical Department, Kazan Federal University, 420008 Kazan, Russia*
[4]*Physical Department, Moscow State University, 119991 Moscow, Russia*

We present infrared spectra of Gd$_2$BaNiO$_5$, which is isostructural to a prototype $S=1$ Haldane compound Y$_2$BaNiO$_5$ containing Ni^{2+} chains, in the spectral range 2 meV–0.55 eV. Unlike Y$_2$BaNiO$_5$, the studied compound contains magnetic rare-earth sublattices and orders antiferromagnetically at $T_N=58$ K. Detailed information on optical phonons is given. Temperature dependences of frequencies and half widths for the two lowest-frequency phonons polarized along the Ni-chain direction evidence the interaction of these lattice vibrations with magnetic excitations. With the help of lattice-dynamics calculations, we find relative displacement vectors of ions for all the phonon modes and use them to discuss the mechanism of phonon-magnon interaction. The optical spectra exhibit a broad absorption continuum for radiation polarized along the chains, probably of magnetic origin, gradually decreasing with lowering temperature. A new mode at about 30 cm^{-1} polarized along the chains (a axis) emerges below $\sim$150 K. A midinfrared absorption peak at 1306 cm^{-1} (0.16 eV) is observed and found to sharpen and shift significantly at T_N. We argue that it can be attributed to a phonon-assisted magnetic absorption and discuss its nature in the framework of the Lorenzana-Sawatzky-Eder model.

I. INTRODUCTION

Gd$_2$BaNiO$_5$ belongs to the family of chain nickelates with a general chemical formula R_2BaNiO$_5$ (R stands for a rare earth or yttrium).[1,2] The most famous member of this family, Y$_2$BaNiO$_5$, is considered as an almost ideal model Haldane spin-1 system.[3] It was Haldane[4] who first recognized the difference in properties of integer-spin and half-integer-spin one-dimensional (1D) Heisenberg antiferromagnetic (HAF) chains. Among these properties, the Haldane gap and finite correlation length for integer-spin 1D HAF chains should be mentioned. Due to structural peculiarities of the chain nickelates, the perfectly straight Ni-O-Ni chains running along the crystallographic a axis form an 1D HAF system of spins $S=1$ (Ni^{2+}, see Fig. 1) with a strong intrachain exchange $J_\parallel \approx 24.6$ meV.[5] The chains are well separated by Ba^{2+} and R^{3+} ions and do not interact magnetically in the case of $R=$Y. As a result, Y$_2$BaNiO$_5$ does not order magnetically down to at least 100 mK (Ref. 6) and demonstrates the Haldane gap $\Delta_H \approx 10$ meV$=80$ cm^{-1}.[3,5,7,8] The presence of magnetic rare-earth ions leads to a certain interchain exchange $J_\perp$ and a long-range magnetic ordering at low temperatures.[2,9–11] In particular, Gd$_2$BaNiO$_5$ first becomes antiferromagnetic at $T_N=58$ K and then undergoes a magnetic reorientation at $T_R=23$ K, where the nickel magnetic moments $\boldsymbol{\mu}_{Ni}$ rotate from the a axis ($\boldsymbol{\mu}_{Ni}\|a$) toward the b axis ($\boldsymbol{\mu}_{Ni}\|b$).[10,12–14] Inelastic neutron-scattering studies of Pr$_2$BaNiO$_5$ and Nd$_2$BaNiO$_5$ (Ref. 11) have revealed well-defined 1D Haldane-gap modes propagating along the Ni chains both *above* and *below* the Néel temperature. Thus, Pr$_2$BaNiO$_5$ and Nd$_2$BaNiO$_5$ preserve 1D properties even at $T<T_N$, due to a small ratio of $J_\perp/J_\parallel$. Such a behavior is expected to be valid for all the other R_2BaNiO$_5$ compounds, e.g., for Gd$_2$BaNiO$_5$ with $J_\perp/J_\parallel \sim 10^{-2}$.[12]

Analytical and numerical Monte Carlo studies of 1D quantum spin chains have demonstrated an essential difference between the spectral density of magnetic excitations as a function of the wave vector in the integer-spin and half-integer-spin 1D systems (see, e.g., Ref. 15). For the spin-1/2 chains, the energy dynamical correlation function was considered and used to calculate the phonon-assisted optical-absorption spectra of magnetic excitations, which turned out to be an asymmetric band with a logarithmic singularity.[16] The calculated line shape reproduced very well infrared (IR) measurements in quasi-1D $S=1/2$ Sr$_2$CuO$_3$.[17] Recently, similar absorption was reported for CuO.[18] As for the integer-spin 1D chains, neither experimental nor theoretical studies of the phonon-assisted magnetic absorption exist up to now, to the best of our knowledge.

One of the aims of the present work is a search for the phonon-assisted magnetic absorption in the quasi-1D $S=1$
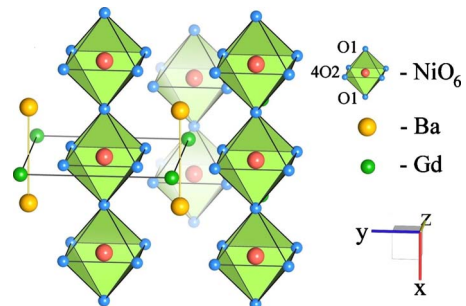

FIG. 1. (Color online) Fragment of the crystal structure of Gd$_2$BaNiO$_5$. The chains of NiO$_6$ corner-sharing octahedra along the a axis are shown, barium and gadolinium being between the chains. The two O1 oxygen atoms of the NiO$_6$ octahedron connect it with other octahedra along the chain, the four O2 atoms lie in the bc plane.

TABLE I. Phonon modes in R_2BaNiO_5.

Atom	Wyckoff position	Site symmetry	Phonon modes
Ni	$2a$ (0 0 0)	D_{2h}	$B_{1u}+B_{2u}+B_{3u}$
Ba	$2c$ (0 0 1/2)	D_{2h}	$B_{1u}+B_{2u}+B_{3u}$
O1	$2b$ (1/2 0 0)	D_{2h}	$B_{1u}+B_{2u}+B_{3u}$
O2$_{1,2}$	$8l$ $(0\ y \pm z)$[a]	C_s (σ^{yz})	$2A_g+A_u+B_{1g}+2B_{1u}+B_{2g}+2B_{2u}+2B_{3g}+B_{3u}$
O2$_{3,4}$	$8l$ $(0\ -y \pm z)$[a]		
Gd$_{1,2}$	$4j$ $(1/2\ 0 \pm z')$[a]	C_{2v} $(C_2^z+\sigma^{xz}+\sigma^{yz})$	$A_g+B_{1u}+B_{2g}+B_{2u}+B_{3g}+B_{3u}$
Total			$3A_g+B_{1g}+2B_{2g}+3B_{3g}+A_u+6B_{1u}+6B_{2u}+5B_{3u}$

[a]$y=0.2414$, $z=0.1479$, and $z'=0.204$ (Ref. 26).

Gd$_2$BaNiO$_5$ compound. The knowledge of phonon modes is essential for such study. Several Raman studies of Gd$_2$BaNiO$_5$ and the parent compound Y$_2$BaNiO$_5$ were reported earlier.[19–22] The assignment of Raman-active modes for the R_2BaNiO_5 $(R=Y,Gd)$ single crystals has been performed,[20] as well as additional modes of magnetic origin have been found.[21] The published data on the IR modes in R_2BaNiO_5 are fragmentary.[22,23] In Ref. 23, the reflectivity spectra of an Y$_2$BaNiO$_5$ single crystal were presented without the analysis of phonon modes.

In this paper we study the temperature-dependent polarized reflectivity spectra of Gd$_2$BaNiO$_5$ in a broad range from 2 meV to 0.55 eV that give us information on the energies, intensities, and linewidths of optical phonons. We use lattice-dynamics calculations to find the eigenvectors of the observed vibrational modes. With the aid of transmission spectroscopy on thin crystals, we get information on weak features in the region of multiphonon absorption which are possibly related to phonon-assisted magnetic transitions.

II. CRYSTAL STRUCTURE AND FACTOR-GROUP ANALYSIS

The crystallographic structure of Gd$_2$BaNiO$_5$ is described by the *Immm* symmetry space group (No. 71). The primitive cell contains nine atoms, which results in 24 vibrational normal modes. Because of the presence of the inversion center, the Raman- and infrared-active modes are separated. Knowing the local symmetry of all the atomic positions, one can perform the factor-group analysis (FGA) to find the symmetries of these modes.[24,25] Though the results of such analysis have already been published in Ref. 19, we show here explicitly which atoms contribute to which vibrational modes, this point being important for the further discussion of the phonon-magnon interaction given in Sec. VI. The atoms, their coordinates in the primitive cell [in units of the lattice constants $a=0.37941$ nm, $b=0.5785$ nm, and $c=1.14121$ nm (Ref. 26)], site symmetries, and modes generated by each position are presented in Table I.

Subtracting the three acoustic modes $B_{1u}+B_{2u}+B_{3u}$ one gets the following optical vibrational modes of the crystal, in accordance with the results of Ref. 19:

$$\Gamma_{vibr} = 3A_g(xx,yy,zz) + B_{1g}(xy) + 2B_{2g}(xz) + 3B_{3g}(yz) + A_u$$
$$+ 5B_{1u}(\boldsymbol{E} \parallel c) + 5B_{2u}(\boldsymbol{E} \parallel b) + 4B_{3u}(\boldsymbol{E} \parallel a)].$$

Notations in parentheses refer to the allowed components of

the electric dipole moment (IR activity) and of the polarizability tensor (Raman activity).

It follows from Table I that only Gd and O2 give rise to the Raman modes while all atoms contribute to the infrared modes. In particular, displacements of nickel and the nearest to Ni oxygen O1 ions contribute only to the IR modes, thus we expect that *only IR modes could show interaction with the excitations of 1D-magnetic chains.*

The lattice normal coordinates corresponding to phonon modes of different symmetries can be written as linear combinations of ion displacements along the crystallographic coordinate axes,

$$Q_i(A_g) = e_{iz}(A_g,R)[z(R_1) - z(R_2)]$$
$$+ e_{iy}(A_g,O2)[y(O2_1) + y(O2_2) - y(O2_3) - y(O2_4)]$$
$$+ e_{iz}(A_g,O2)[z(O2_1) - z(O2_2) + z(O2_3) - z(O2_4)],$$

$$Q(B_{1g}) = [x(O2_1) + x(O2_2) - x(O2_3) - x(O2_4)]/2,$$

$$Q(A_{2u}) = [x(O2_1) - x(O2_2) - x(O2_3) + x(O2_4)]/2,$$

$$Q_i(B_{2g}) = e_{ix}(B_{2g},R)[x(R_1) - x(R_2)]$$
$$+ e_{ix}(B_{2g},O2)[x(O2_1) - x(O2_2) + x(O2_3) - x(O2_4)],$$

$$Q_i(B_{3g}) = e_{iy}(B_{3g},R)[y(R_1) - y(R_2)]$$
$$+ e_{iy}(B_{3g},O2)[y(O2_1) - y(O2_2) + y(O2_3) - y(O2_4)]$$
$$+ e_{iz}(B_{3g},O2)[z(O2_1) + z(O2_2) - z(O2_3) - z(O2_4)],$$

$$Q_i(B_{1u}) = e_{iz}(B_{1u},R)[z(R_1) + z(R_2)]$$
$$+ e_{iz}(B_{1u},O2)[z(O2_1) + z(O2_2) + z(O2_3) + z(O2_4)]$$
$$+ e_{iz}(B_{1u},Ba)z(Ba) + e_{iz}(B_{1u},Ni)z(Ni)$$
$$+ e_{iz}(B_{1u},O1)z(O1) + e_{iy}(B_{1u},O2)[y(O2_1)$$
$$- y(O2_2) - y(O2_3) + y(O2_4)],$$

$$Q_i(B_{2u}) = e_{iy}(B_{2u},R)[y(R_1) + y(R_2)]$$
$$+ e_{iy}(B_{2u},O2)[y(O2_1) + y(O2_2) + y(O2_3) + y(O2_4)]$$
$$+ e_{iy}(B_{2u},Ba)y(Ba) + e_{iy}(B_{2u},Ni)y(Ni)$$
$$+ e_{iy}(B_{2u},O1)y(O1) + e_{iz}(B_{2u},O2)[z(O2_1)$$
$$- z(O2_2) - z(O2_3) + z(O2_4)],$$

$$Q_i(B_{3u}) = e_{ix}(B_{3u},R)[x(R_1) + x(R_2)]$$
$$+ e_{ix}(B_{3u},O2)[x(O2_1) + x(O2_2) + x(O2_3) + x(O2_4)]$$
$$+ e_{ix}(B_{3u},Ba)x(Ba) + e_{ix}(B_{3u},Ni)x(Ni)$$
$$+ e_{ix}(B_{3u},O1)x(O1).$$

The components of the phonon polarization vectors $e_{i\alpha}(\Gamma,\lambda)$ can be obtained as the normalized eigenvectors of a lattice dynamical matrix at the Brillouin-zone center.

III. SAMPLES AND THE OPTICAL EXPERIMENT

Single crystals of Gd_2BaNiO_5 were grown by the floating-zone technique in an image furnace, as described in Ref. 27. Their microstructure was checked by electron microscopy and optical microscopy in polarized light. The composition of the grown crystals was determined by energy-dispersive x-ray spectroscopy analyses and the crystal structure verified with the aid of x-ray powder-diffraction patterns taken using Cu $K\alpha$ radiation.[27] Single crystals had typical dimensions $3 \times 3 \times 3$ mm^3 and were oriented using the x-ray diffraction method. For different optical measurements we prepared samples of various thicknesses. The crystal surface in all cases was polished using diamond abrasive with the finesse down to 0.1 μm.

Temperature-dependent reflection and transmission spectra in the spectral range from 20 to 4400 cm^{-1} (2.5 meV–0.55 eV) and the temperature interval from 7 to 300 K were measured for $E\|a$, $E\|b$, and $E\|c$ polarizations of the incident light, using a Fourier spectrometer Bruker 113 and a helium flow cryostat. The reflectivity was obtained on the thickest samples, in order to diminish internal reflections. However, the Fabry-Perot oscillations were still noticeable due to the completely insulating nature of this compound. *In situ* gold evaporation was used in order to obtain the absolute reflectivity. The transmission spectra were measured on thinner samples.

IV. EXPERIMENTAL RESULTS

Figures 2(a) and 3(a) show the reflection spectra at 300 and at 7 K for two polarizations, parallel ($E\|a$) and, respectively, perpendicular ($E\|c$) to the chains. The optical conductivity for both polarizations [Figs. 2(b) and 3(b)] was obtained by a Kramers-Kronig constrained variational analysis,[28] which takes into account the Fabry-Perot interference fringes due to multiple internal reflections. Nevertheless, small oscillations still remain in the optical conductivity spectra. Four strong phonons for the $E\|a$ polarization and five ones for each of the $E\|b$ (not shown) and $E\|c$ polarizations are present, which is in accordance with the results of FGA. The dips in optical conductivity right below the strong phonon peaks at 51 and 185 cm^{-1} for the polarization $E\|a$ are likely to be artifacts of the variational analysis, related to the difficulty of a precise fitting of the Fabry-Perot interference. The phonons shift and narrow markedly with cooling down. One can also see that the Fabry-Perot interference fringes at low frequencies (below 150 cm^{-1}) become more pronounced at 7 K as compared to room temperature. Al-
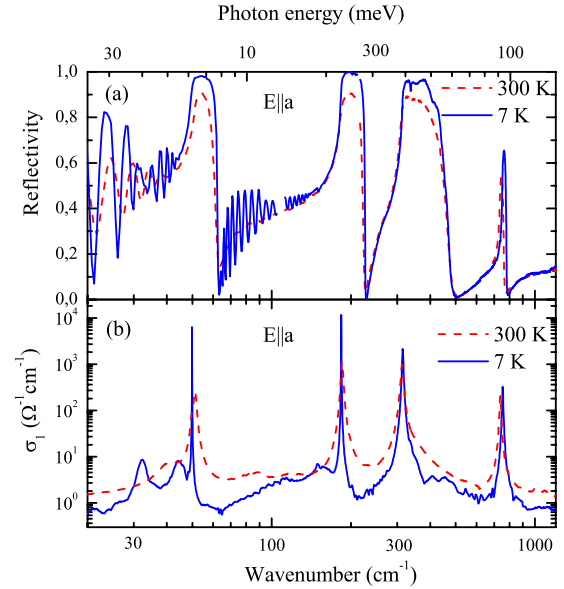

FIG. 2. (Color online) (a) Reflectivity and (b) optical conductivity σ_1 of Gd_2BaNiO_5 along the chains ($E\|a$), at room temperature and at 7 K. One can clearly see an enhancement of the interference pattern in the low-frequency part of the reflectivity spectrum and the corresponding diminishing of the low-frequency optical conductivity.

though this effect can be partially related to the narrowing of the phonon modes, leading to a higher transparency at low temperatures, we note that temperature dependence of the Fabry-Perot oscillations is much stronger for the polarization $E\|a$ (along the chains). This implies that there is an extra optical absorption related to spin dynamics, which shows a significant temperature dependence.

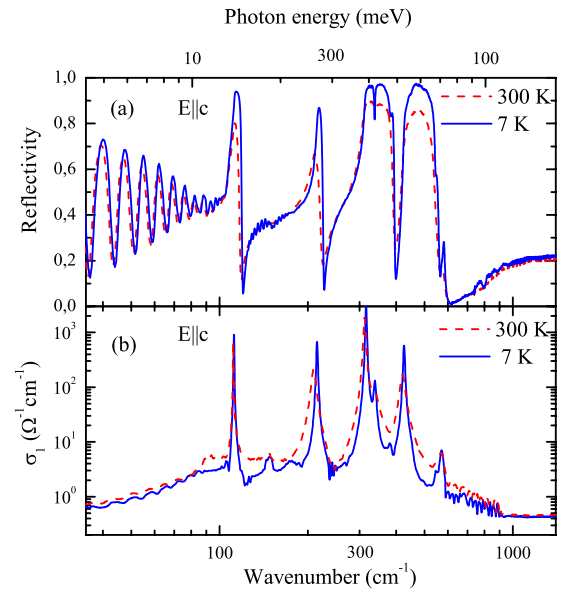In Table II we present the frequencies of the infrared modes of Gd_2BaNiO_5 at 300 K. The phonon parameters for

FIG. 3. (Color online) (a) Reflectivity and (b) optical conductivity σ_1 of Gd_2BaNiO_5 perpendicular to the chains ($E\|c$), at room temperature and at 7 K.

TABLE II. Measured and calculated frequencies ω_i (cm^{-1}) and half widths γ (cm^{-1}) of the IR and Raman-active phonons (Raman experimental frequencies from Ref. 20) in Gd$_2$BaNiO$_5$ at room temperature. Frequencies of the corresponding vibrations in Y$_2$BaNiO$_5$ are in brackets (Refs. 20 and 23).

IR modes					Raman modes	
Experiment			Theory		Experiment[a]	Theory
ω_{TO}	ω_{LO}	γ	ω_{TO}	ω_{LO}	ω	
B_{3u} ($E\|a$)					A_g	
51 (-)	62 (-)	1.3	84	85	175 (233)	151
185 (208)	225 (239)	3.6	163	177	518 (540)	479
313 (321)	473 (486)	7.6	303	562	562 (584)	582
739 (759)	764 (790)	10.7	735	760	B_{1g}	
B_{2u} ($E\|b$)					335 (340)	294
96 (112)	98 (117)	9	112	114	B_{2g}	
130 (134)	146 (152)	11	170	178	123 (160)	120
284 (286)	340 (346)	7	257	297	312 (328)	343
382 (398)	474 (-)	16	369	491	B_{3g}	
486 (-)	549 (568)	25	492	617	183 (184)	179
B_{1u} ($E\|c$)					204 (269)	228
110 (115)	118 (122)	3	123	137	422 (440)	426
208 (219)	222 (244)	9	238	246		
312 (347)	394 (403)	6	332	373		
421 (427)	555 (552)	19	382	575		
566 (570)	582 (605)	35	595	634		

[a]Reference 20.

each polarization were extracted from the reflectivity spectra using a general model of anisotropic Drude-Lorentz oscillators. The TO frequencies correspond to the peaks of the optical conductivity [Figs. 2(b) and 3(b)], the LO frequencies were found from the spectrum of the loss function Im[
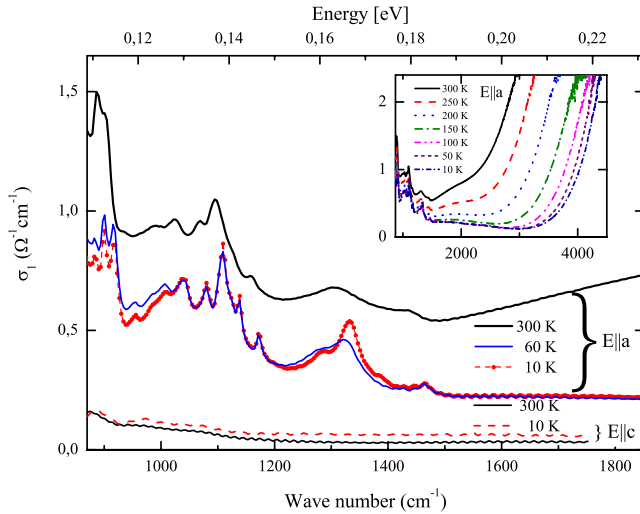

FIG. 4. (Color online) Optical conductivity of Gd$_2$BaNiO$_5$ at several temperatures above and below T_N=58 K, in the midinfrared region. Inset displays an extended spectral region demonstrating the onset of the nickel *d-d* transitions for optical conductivity along the chains and a considerable temperature shift of the *d-d* optical-absorption edge.

$-1/\varepsilon(\omega)$] (not shown). To complete the experimental data on phonon parameters (Table II), we added the data on Raman frequencies at room temperature.[20]

In the spectral region between 900 and 4000 cm^{-1}, additional weak absorption peaks are present, mostly for the polarization along the chains ($E\|a$). To analyze these modes, we have studied temperature-dependent transmission spectra in the mentioned region. The optical conductivity calculated from these spectra is presented in Fig. 4. The optical conductivity peaks demonstrate gradual shift and narrowing while cooling from 300 K to low temperatures. Meanwhile, we would like to note that between 60 K ($T>T_N$) and 10 K ($T<T_N$) only one mode (1306 cm^{-1} at 300 K, see Fig. 4) substantially changes its position. The absorption above 2000 cm^{-1} is due to the *d-d* transitions in the Ni^{2+} ion (see, e.g., Ref. 29). It decreases with lowering the temperature due to the narrowing and shift of the *d-d* absorption bands. This effect is much more pronounced in the $E\|a$ spectra where the *d-d* absorption edge (shown in the inset of Fig. 4) is situated at lower frequencies than for $E\|c$. Our data on the Ni^{2+} *d-d* absorption edge in Gd$_2$BaNiO$_5$ are in agreement with the data of Ref. 30 on the Ni^{2+} *d-d* optical absorption in Y$_2$BaNiO$_5$.

V. LATTICE-DYNAMICS CALCULATIONS

The calculation of lattice dynamics for Gd$_2$BaNiO$_5$ was performed in the framework of the rigid-ion model, which allows for the long-range (Coulomb) and short-range (non-

TABLE III. Ion charges (in units of the proton charge) and parameters of the non-Coulomb interactions in Gd_2BaNiO_5 (in units of joules per square meter).

Ion	Charge	Bond type and length, R (nm)	$\frac{1}{R}\frac{dV}{dR}$	$\frac{d^2V}{dR^2}$	Bond type and length, R (nm)	$\frac{1}{R}\frac{dV}{dR}$	$\frac{d^2V}{dR^2}$
Ni	0.94	Ni-O1 0.1897	−30	241	O1-O2 0.2898	−0.8	7.5
Ba	1.58	Ni-O2 0.2191	−14	125	O2-O2 0.2793	−1	8
Gd	2.16	Gd-O2 0.2257	−20	150	O2-O2 0.3006	−0.5	4.5
O1	−1.04	Gd-O1 0.2328	−15	130	Ba-O1 0.2892	−12	98
O2	−1.45	Gd-O2 0.2441	−14	113	Ba-O2 0.2947	−8	55

Coulomb) interactions between the ions. The energy of the non-Coulomb interactions was modeled as a function $V(R)$ of the distance R between the ions. The contributions to the lattice force constants determined by the first and second derivatives of the function $V(R)$ were taken into account and considered as model parameters. Lattice sums in the Coulomb terms were calculated by making use of the Ewald method. The effective ion charges and the first and second derivatives of the functions $V(R)$ for different pairs of the interacting ions (see Table III) were obtained by fitting the calculated phonon frequencies to the results of measurements (see Table II). The effective charge of the oxygen O1 ions is well defined by the LO-TO splitting of high-frequency B_{3u} mode (764–739 cm^{-1}). A large difference between the nominal and effective charges (for example, −2 and −1.04 for the O1 ions) can be explained by a strong covalent character of the Ni-O1 bonds which correlates with a strong exchange interaction between the nearest-neighbor Ni ions through the intermediate O1 ions. The calculated frequency of the silent mode A_{2u} in Gd_2BaNiO_5 equals 228 cm^{-1}. The elastic constants of Gd_2BaNiO_5 estimated from the calculated sound velocities along the crystallographic axes are $C_{11}=281$ GPa, $C_{22}=311$ GPa, $C_{33}=218$ GPa, $C_{44}=68.5$ GPa, $C_{55}=52.4$ GPa, and $C_{66}=32.5$ GPa.

Although we could not achieve a perfect agreement between the experimental and calculated frequencies using physically reasonable parameters (which is not surprising given the simplicity of the lattice-dynamical model used), the calculations reproduce correctly the main principal features of the phonon spectra in R_2BaNiO_5 and give us relative displacement vectors of ions for all the phonon modes. Table IV lists the calculated components of the polarization vectors in Gd_2BaNiO_5 but Fig. 5 illustrates atomic movements in the unit cell for different IR phonon modes.

Raman modes are generated by the displacements of only two atoms (Gd and O2). Moreover, the lowest-frequency A_g, B_{2g}, and B_{3g} modes involve mainly the gadolinium vibrations which leads to a well pronounced dependence of the phonon frequency on the ionic mass (Gd vs Y). The infrared-active modes, in general, include displacements of all the atoms and therefore have a complex nature. Nevertheless, among these modes the B_{3u}-TO mode at 739 cm^{-1} has a specific character as it contains mostly the in-chain vibrations of the Ni and O1 atoms As it is discussed below, this makes favorable a coupling of this mode to magnetic excitations. The other three B_{3u} modes also modulate the Ni-O distances along the chains, although in a less degree than the mode at 739 cm^{-1}.

VI. DISCUSSION

The most striking feature of the optical conductivity of Gd_2BaNiO_5 is, probably, the existence of the low-frequency continuum in the $E\|a$ polarization and an opening of the optical gap with lowering the temperature. Figure 6 shows the temperature dependence of the in-chain optical conductivity at two selected frequencies (80 and 200 cm^{-1}) away from the phonon peaks. The curves clearly show a kink near the Neel temperature. This fact suggests that the background is due to a broadband magnetic absorption. Simultaneously with the optical gap opening, a new mode at about 30 cm^{-1} emerges and becomes visible below ~200 K (see Fig. 7). Before discussing the origin of the observed optical absorption continuum and the new mode 30 cm^{-1}, we briefly review the known data on the magnetic excitations of quantum spin chains.

Magnetic excitations of the 1D HAF chains were intensely studied both theoretically[15,31] and experimentally.[8,32,33] Any *isolated* 1D magnetic chain does not order magnetically even at zero temperature because of quantum fluctuations. There is, however, a fundamental difference between the integer- and half-integer-spin chains:[4] an integer-spin chain possesses sites with zero spin projection and, as a consequence, has a gap in the spectrum of magnetic excitations (the Haldane gap) and exponentially decaying spin correlations (in contrast to a power law in the $S=1/2$ case). At zero temperature, in the higher wave vector region $q>\pi/2a$ (a is the lattice constant which equals to the distance between the Ni spins in the chain) the magnetic excitations are well defined quasiparticles but in the wave-vector region $0\leq q<\pi/3a$ they are two-particle excitations where both constituent particles are taken from $q\approx\pi/a$ region.[15] The Haldane gap at $q=\pi/a$ has the value $\Delta_H=0.41J_\|$ and, correspondingly, the lower boundary of the two-particle continuum at $q=0$ is at $2\Delta_H$.[15] The evolution of the magnetic excitation spectral density shape from a narrow peak at $q=\pi/a$ to a smeared continuum near $q=0$ is continuous and monotonic. A rather narrow spectral distribution is still observed at $q=\pi/2a$, peaked near the maximum of the spin-wave dispersion curve $E(q=\pi/2a)=2J_\|\sqrt{S(S+1)}$.[15,34] At elevated temperatures, the gap shifts to higher energies and spreads while the dispersion curves flatten.[32] In Y_2BaNiO_5, the Haldane gap becomes overdamped and the corresponding neutron scattering peak is no longer observed above ~100 K, which is the order of the energy gap.[8] Below the temperature of the three-dimensional (3D) magnetic order-

TABLE IV. Polarization vector components $e_{i\alpha}$ (TO,λ) for optical phonons in Gd$_2$BaNiO$_5$, indicated by their symmetry and the measured frequency (in cm^{-1}, see Table II).

		IR modes						Raman modes		
		B_{1u}						A_g		
λ α	110	208	312	421	566	λ α	175	518	562
R z	0.2150	−0.4049	−0.1490	0.0356	−0.0086	R z	$\sim 1/\sqrt{2}$	~ 0	~ 0
Ba z	−0.8579	0.1669	−0.0073	0.0538	−0.0250	O2 z	~ 0	0.289	0.407
Ni z	0.3349	0.7499	−0.4256	0.1811	0.1104	O2 y	~ 0	−0.407	0.289
O1 z	0.1300	0.0716	0.6918	0.6140	0.3086				
O2 z	0.0984	0.1354	0.2698	−0.3354	−0.0982				
O2 y	0.0304	0.0295	0.0343	0.1836	−0.4618				
		B_{2u}						B_{3g}		
λ α	96	130	284	382	486	λ α	183	204	422
R y	−0.4451	0.0731	0.1544	−0.0796	0.0088	R y	$\sim 1/\sqrt{2}$	~ 0	~ 0
Ba y	0.4604	−0.6934	−0.0607	−0.1807	0.1959	O2 y	~ 0	0.448	0.221
Ni y	0.5827	0.6466	0.1585	−0.3256	−0.1085	O2 z	~ 0	−0.221	0.448
O1 y	0.1482	−0.1598	0.2515	0.4921	−0.7874				
O2 y	0.0443	0.1236	−0.3364	0.2900	0.0915				
O2 z	0.0747	0.0309	0.3192	0.2598	0.2721				
		B_{3u}					B_{2g}		B_{1g}	
λ α	51	185	313	739		λ α	123	312	335
R x	0.3329	0.3213	0.1403	−0.0014		R x	$\sim 1/\sqrt{2}$	~ 0	
Ba x	−0.8652	0.0706	0.1172	−0.0115		O2 x	~ 0	~ 0.5	0.5
Ni x	0.1469	−0.7889	0.3027	0.4062					
O1 x	0.0797	−0.3704	0.0448	−0.9096					
O2 x	0.0217	−0.0849	−0.4619	0.0435					

ing, the Haldane gap and the in-chain magnetic excitations still survive although their spectral weight is redistributed in favor of the emergent 3D magnons.[11,32] With three magnetic ions (Ni+2Gd) per crystallographic primitive cell of Gd$_2$BaNiO$_5$ and six per magnetic cell, a number of 3D magnon branches may be expected, most of them in the energy region $\sim \sqrt{J_\parallel J_\perp} \approx 2.5$ meV $= 20$ cm^{-1}. As far as we know, there are no experimental data on these low-energy magnons.

At the first glance, the observed low-frequency optical-absorption continuum at elevated temperatures $T > \Delta_H$ could be connected with the creation by the photon (which has the wave vector $q \approx 0$) of the Haldane chain spin excitation with the wave vector $q = 0$ or a pair of spin excitations with wave vectors q and $-q$. However, such absorption would start above $\sim 2\Delta_H \approx 160$ cm^{-1}. Even more important, the absorption associated with one spin[35] is symmetry forbidden, because the local symmetry group of Ni^{2+} contains inversion, and so is the two-magnon optical absorption that might be induced by exchange interactions within the chains, because of the presence of the center of inversion at the half distance between the two neighboring Ni ions along the chain.[35] The exchange mechanism should, however, be effective for the AF spin pairs in the neighboring chains within the ab plane and along the c axis. Possibly, the low-frequency background and the new mode 30 cm^{-1} are connected with the two-magnon optical absorption within the ab planes. Magnetic correlations in these planes persist well above $T_N = 58$ K giving rise to a broad low-frequency background absorption, which gradually transforms into a well-defined peak with decreasing the temperature.

To get a deeper insight into a possible interaction of lattice vibrations with magnetic excitations, in Figs. 8 and 9 we have plotted the temperature dependence of the TO frequencies and half widths of the infrared-active modes polarized along the a and c axes, respectively. The two lowest-frequency vibrations along the chain direction, namely, the B_{3u} modes 51 and 185 cm^{-1} *soften* with lowering the temperature while the other infrared (and Raman[21]) active modes exhibit a more conventional hardening with cooling down (which corresponds to the hardening of atomic bonds with diminishing interatomic distances). The same two modes show the strongest narrowing with lowering the temperature. The ratios of the half widths at $T = 5$ K and at room temperature for these vibrational modes are less than 0.1, in contrast
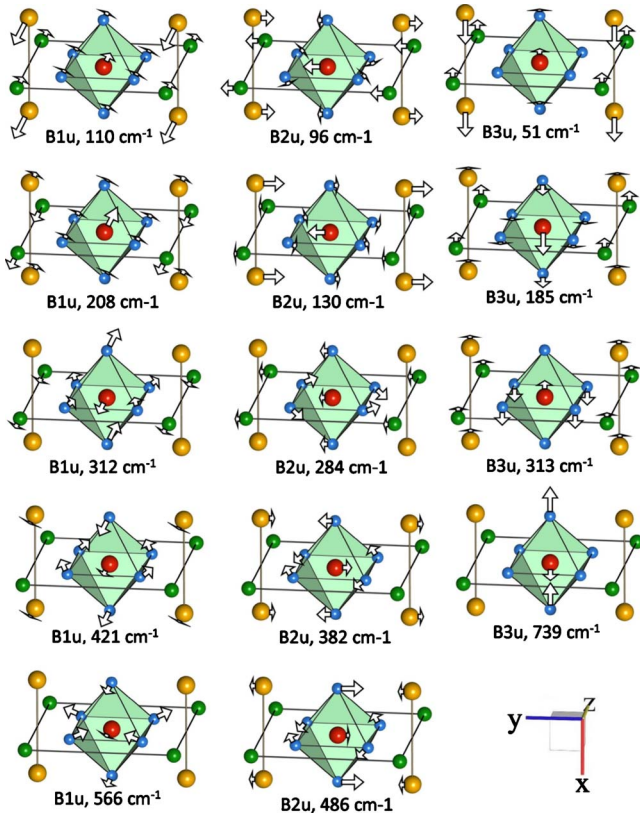
FIG. 5. (Color online) IR-active phonons in Gd_2BaNiO_5: schematic view of polarization vectors found from lattice-dynamics calculations. Symmetries and measured phonon frequencies are indicated.

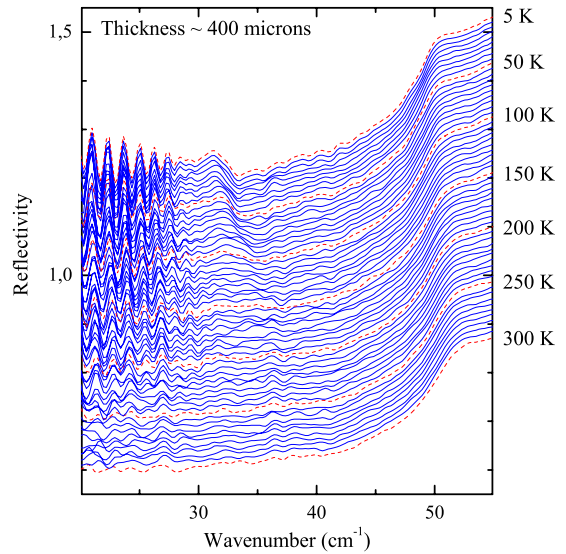FIG. 7. (Color online) Emergence of a new mode at 30 cm^{-1}. Reflectivity curves at different temperatures are shifted successively along the y axis.

to the values between 0.3 and 0.7 found for other vibrations. Such behavior of the in-chain modes 51 and 185 cm^{-1} could be connected to the interaction of these lattice vibrations with spin fluctuations within the system of interacting Ni-O-Ni antiferromagnetic chains.

To discuss the mechanism of the interaction between the in-chain lattice vibrations and the magnetic excitations, we inspect the eigenvectors of the in-chain (B_{3u}) modes, found from the lattice dynamics calculations (see Table IV). In all the B_{3u} modes the atomic displacements are along the a axis. In particular, these modes modulate the lengths of the Ni-O-Ni bonds along the chain and, thus, the Ni-Ni exchange integral. The strongest modulation is realized in the 739 cm^{-1} B_{3u} mode, then come the 185, 313, and 51 cm^{-1} B_{3u} modes. Being in resonance with the magnetic two-particle continuum, a phonon of the Brillouin-zone center

FIG. 6. (Color online) Temperature dependences of background optical conductivity along the chain direction for the two selected wave numbers, 80 and 220 cm^{-1}. A kink near the Neel temperature is seen.
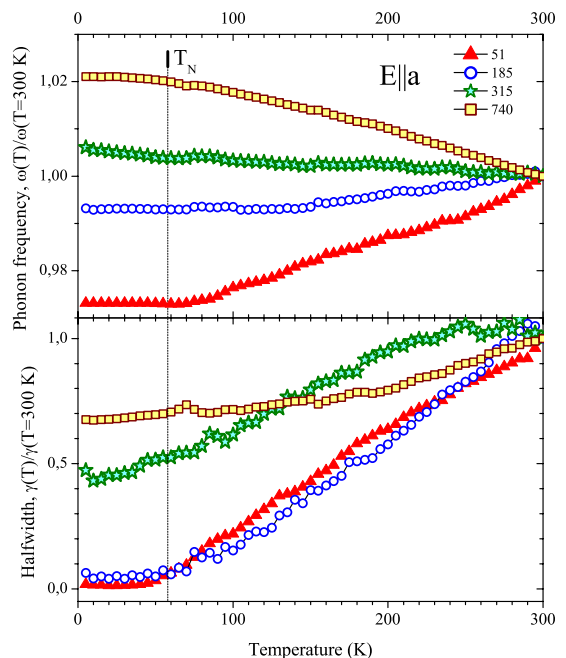

FIG. 8. (Color online) Temperature dependence of the relative frequencies and half widths of the B_{3u} TO vibrations along the chains.
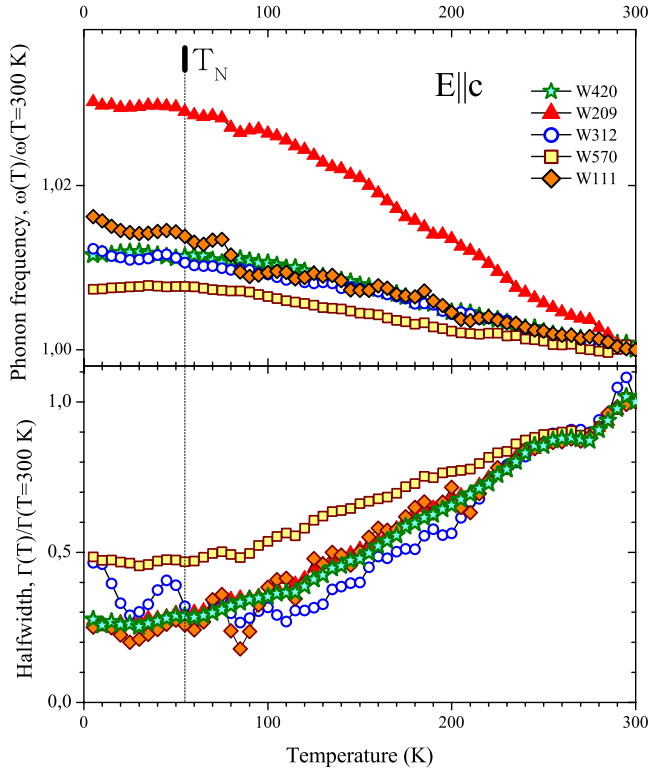
FIG. 9. (Color online) Temperature dependence of the relative frequencies and half widths of the IR-active phonons polarized perpendicular to the chains.
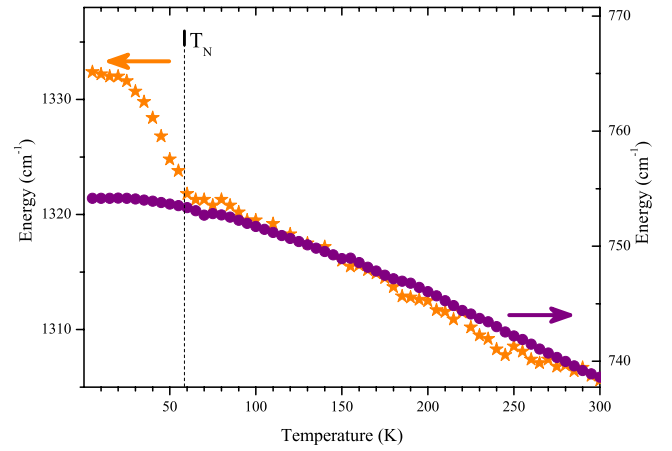

FIG. 10. (Color online) Temperature dependence of the peak near 1306 cm^{-1} compared to the temperature dependence of the B_{3u} TO phonon frequency near 740 cm^{-1}.

broadens and shifts due to a decay into two magnetic excitations with opposite directions of the wave vectors, q and $-q$. The largest density of the in-chain magnetic excitations is concentrated at $q = \pi/a$ in the Haldane-gap mode. In the family of compounds $(Nd_xY_{1-x})_2BaNiO_5$, the Haldane-gap mode was found to smoothly shift from 80 to 92.5 cm^{-1} (which is half the frequency of the 185 cm^{-1} B_{3u} mode) in the temperature interval from 50 to 80 K.[36] Softening and narrowing of the 185 cm^{-1} B_{3u} mode with decreasing the temperature can be related to a corresponding diminishing of the spectral width for magnetic excitations and a redistribution of the spectral weight.

This scenario is not fit for the mode 51 cm^{-1} half the frequency of which is well within the Haldane gap. However, both the mode 51 cm^{-1} and the mode 185 cm^{-1} are in resonance with the broad low-frequency continuum at elevated temperatures, which was tentatively assigned to the two-magnon optical absorption due to magnetic fluctuations within the *ab* planes. Both discussed modes strongly modulate the exchange interaction between the Ni ions in neighboring chains within the *ab* plane, by modulating the Ni-O2-O2-Ni and Ni-O2-Gd-O2-Ni angles and, thus, interact with the in-plane magnetic excitations. Just this mechanism could give the main contribution to the broadening of the mode 51 cm^{-1} at elevated temperatures. It seems possible that, at low temperatures, the continuum transforms into the well-defined peak 30 cm^{-1} of the two-magnon absorption and the modes 51 and 185 cm^{-1} go out of the resonance.

As for the B_{3u} modes 739 and 313 cm^{-1}, their decay is hindered because halves their frequencies are in the region of

very low density of the magnetic excitations.[8] We argue below that the mode 739 cm^{-1}, which the most strongly modulates the exchange interaction within Ni-O-Ni chains, manifests its interaction with the in-chain magnetic fluctuations in a different way, by a peculiar spectral feature in the mid-IR (MIR) spectral region.

Multiple peaks are observed in the in-chain $E\|a$ absorption spectra above the optical-phonon frequencies (see Fig. 4). The analysis of the peak frequencies and their temperature dependences shows that most of the MIR peaks are due to the two-phonon absorption. However, the peak at about 1306 cm^{-1} (at room temperature) falls out of this interpretation. Figure 10 shows the temperature dependences of the frequency of this peak, together with the frequency of the vibrational mode near 739 cm^{-1} exhibiting the largest observed frequency shift. It is evident that the frequency of the considered peak 1306 cm^{-1} has a peculiarity at the temperature of the magnetic ordering $T_N = 58$ K while the mode 739 cm^{-1} (as well as any other vibrational mode) does not have any. This fact points to the magnetic nature of the optical-absorption peak at 1306 cm^{-1}. We tentatively assign this feature to the phonon-assisted absorption by magnetic excitations of the $S=1$ HAF nickel chains. Similar absorption by spinons of $S=1/2$ copper chains has been observed in Sr_2CuO_3,[17] and, recently, in CuO both above and below T_N.[18] It has been shown that the peak frequency equals $\omega_0 + E(q = \pi/2a)$, where ω_0 is the frequency of vibration that strongly modulates the Cu-O-Cu distances along the chain but $E(q = \pi/2a)$ is the energy at the lower boundary of the spinon continuum at $q = \pi/2a$, $E(q = \pi/2a) = \pi J/2$. The wave vector of magnetic excitation needs not be zero because of the phonon recoil.[17] Dispersion of a high-frequency optical phonon, which is much smaller than the typical energy scale of the spin system, $J_\|$, can usually be neglected.[17] A comprehensive theory exists now for the $S=1/2$ (half-integer-spin) HAF chains.[16,37,38] We suppose that a similar mechanism should exist for the $S=1$ (integer-spin) HAF chains, resulting in phonon-assisted magnetic absorption with a peak frequency equal to $\omega_0 + E(q = \pi/2a) \approx \omega_0 + 2J\sqrt{S(S+1)}$. In particular, for Gd_2BaNiO_5, as it follows from vibrational eigen-

vectors, the Ni-O-Ni distances along the nickel chains are the most strongly modulated by the B_{3u} TO vibration with the frequency of $\omega_0 = 739$ cm^{-1}. The frequency of the highest B_{3u} LO mode (764 cm^{-1}) monotonously diminishes with the increasing propagation vector along the HAF chains and, in particular, according to calculations, equals 747 cm^{-1} for the phonon wave vector $(\pi/2a, 0, 0)$. Also, it should be noted that the calculated phonon density of states in Gd$_2$BaNiO$_5$ contains a narrow peak at the frequency ω_0. Taking the value $J_\parallel = 198$ cm^{-1} as for Y$_2$BaNiO$_5$,[5] we obtain $E(q = \pi/2a) \approx 2J\sqrt{S(S+1)} = 560$ cm^{-1} which results in $\omega_0 + E(q = \pi/2a) \approx 1300$ cm^{-1}, close to the observed peak frequency 1306 cm^{-1}. It should be noted that the MIR band at 0.25 eV observed in the absorption spectra of La$_2$NiO$_4$ has been qualitatively described by a two-dimensional version[37] of the already mentioned theory of the phonon-assisted magnon absorption.[16]

VII. SUMMARY

Polarized temperature-dependent reflection spectroscopy of Gd$_2$BaNiO$_5$ single crystal and lattice-dynamics calculations allowed us to sort out three phonons of the B_{3u} symmetry (51, 185, and 739 cm^{-1}) that modulate exchange interactions between the nearest-neighbor Ni ions within the magnetic 1D chains and between the Ni ions in neighboring chains. Two of them, at 51 and 185 cm^{-1}, demonstrate an unusual temperature behavior of the frequency and half width. We attribute such behavior to the interaction of these modes with a continuum of magnetic excitations. The third mode (739 cm^{-1}) gives rise to the strongest modulation of the Ni-Ni exchange and activates the magnetic absorption (so-called phonon-assisted magnetic absorption) which results in a broad band in the region of two-phonon absorption, distinguished by a peculiarity in its spectral position at T_N. The energy of this band corresponds to the sum of the phonon energy and the energy at the lower boundary of the spinon continuum at $q = \pi/2a$. A new mode at about 30 cm^{-1} polarized along the chains (a axis) was found and tentatively attributed to the two-magnon absorption due to the AF spin pairs in the neighboring chains within the ab plane.

ACKNOWLEDGMENTS

[1] S. Schiffler and H. Müller-Buschbaum, Z. Anorg. Allg. Chem. **532**, 10 (1986).

[2] J. A. Alonso, J. Amador, J. L. Martínez, I. Rasines, J. Rodríguez-Carvajal, and R. Sáez-Puche, Solid State Commun. **76**, 467 (1990).

[3] G. Xu, J. F. DiTusa, T. Ito, K. Oka, H. Takagi, C. Broholm, and G. Aeppli, Phys. Rev. B **54**, R6827 (1996).

[4] F. D. M. Haldane, Phys. Rev. Lett. **50**, 1153 (1983).

[5] J. Darriet and L. P. Regnault, Solid State Commun. **86**, 409 (1993).

[6] K. Kojima, A. Keren, L. P. Le, G. M. Luke, B. Nachumi, W. D. Wu, Y. J. Uemura, K. Kiyono, S. Miyasaka, H. Takagi, and S. Uchida, Phys. Rev. Lett. **74**, 3471 (1995).

[7] T. Yokoo, T. Sakaguchi, K. Kakurai, and J. Akimitsu, J. Phys. Soc. Jpn. **64**, 3651 (1995).

[8] T. Sakaguchi, K. Kakurai, T. Yokoo, and J. Akimitsu, J. Phys. Soc. Jpn. **65**, 3025 (1996).

[9] G. G. Chepurko, Z. A. Kazei, D. A. Kudrjavtsev, R. Z. Levitin, B. V. Mill, M. N. Popova, and V. V. Snegirev, Phys. Lett. A **157**, 81 (1991).

[10] E. García-Matres, J. L. García-Muñoz, J. L. Martínez, and J. Rodríguez-Carvajal, J. Magn. Magn. Mater. **149**, 363 (1995).

[11] A. Zheludev, J. M. Tranquada, T. Vogt, and D. J. Buttrey, Phys. Rev. B **54**, 6437 (1996); **54**, 7210 (1996).

[12] A. Butera, M. T. Causa, M. Tovar, S. B. Oseroff, and S.-W. Cheong, J. Magn. Magn. Mater. **140-144**, 1681 (1995).

[13] M. N. Popova, I. V. Paukov, Yu. A. Hadjiiski, and B. V. Mill, Phys. Lett. A **203**, 412 (1995).

[14] G. A. Stewart, S. J. Harker, M. Strecker, and G. Wortmann, Phys. Rev. B **61**, 6220 (2000).

[15] S. V. Meshkov, Phys. Rev. B **48**, 6167 (1993).

[16] J. Lorenzana and R. Eder, Phys. Rev. B **55**, R3358 (1997).

[17] H. Suzuura, H. Yasuhara, A. Furusaki, N. Nagaosa, and Y. Tokura, Phys. Rev. Lett. **76**, 2579 (1996).

[18] SeongHoon Jung, Jooyeon Kim, E. J. Choi, Y. Sekio, T. Kimura, and J. Lorenzana, Phys. Rev. B **80**, 140516 (2009).

[19] A. de Andres, J. L. Martinez, R. Saez-Puche, and A. Salines-Sanchez, Solid State Commun. **82**, 931 (1992).

[20] P. E. Sulewski and S.-W. Cheong, Phys. Rev. B **50**, 551 (1994).

[21] P. E. Sulewski and S.-W. Cheong, Phys. Rev. B **51**, 3021 (1995).

[22] N. Ogita, Y. Tsunezumi, T. Yokoo, J. Akimitsu, and M. Udagawa, J. Phys. Soc. Jpn. **66**, 873 (1997).

[23] T. Ito, H. Yamaguchi, K. Oka, K. M. Kojima, H. Eisaki, and S. Uchida, Phys. Rev. B **64**, 060401 (2001).

[24] B. N. Mavrin, Optika i Spektroskopiya **49**, 79 (1980).

[25] D. L. Rousseau, R. P. Bauman, and S. P. S. Porto, J. Raman Spectrosc. **10**, 253 (1981).

[26] E. García-Matres, J. L. Martínez, J. Rodríguez-Carvajal, J. A. Alonso, A. Salinas-Sanchez, and R. Saez-Puche, J. Solid State Chem. **103**, 322 (1993).

[27] M. N. Popova, S. A. Klimin, P. Higel, and G. Dhalenne, Phys. Lett. A **354**, 487 (2006).

[28] A. B. Kuzmenko, Rev. Sci. Instrum. **76**, 083108 (2005).

[29] T. Tsuboi and W. Kleemann, J. Phys.: Condens. Matter **6**, 8625 (1994).

[30] R. Rückamp, E. Benckiser, M. W. Haverkort, H. Roth, T. Lorenz, A. Freimuth, L. Jongen, A. Möller, G. Meyer, P. Reutler, B. Büchner, A. Revcolevschi, S.-W. Cheong, C. Sekar, G. Krab-

bes, and M. Grüninger, New J. Phys. **7**, 144 (2005).

[31] G. Gómez-Santos, Phys. Rev. Lett. **63**, 790 (1989).

[32] M. Kenzelmann, R. A. Cowley, W. J. L. Buyers, R. Coldea, J. S. Gardner, M. Enderle, D. F. McMorrow, and S. M. Bennington, Phys. Rev. Lett. **87**, 017201 (2001); M. Kenzelmann, R. A. Cowley, W. J. L. Buyers, and D. F. McMorrow, Phys. Rev. B **63**, 134417 (2001); M. Kenzelmann, R. A. Cowley, W. J. L. Buyers, Z. Tun, R. Coldea, and M. Enderle, *ibid.* **66**, 024407 (2002).

[33] I. A. Zaliznyak, S.-H. Lee, and S. V. Petrov, Phys. Rev. Lett. **87**, 017202 (2001).

[34] G. Xu, G. Aeppli, M. E. Bisher, C. Broholm, J. F. DiTusa, C. D. Frost, T. Ito, K. Oka, R. L. Paul, H. Takagi, and M. M. J. Treacy, Science **289**, 419 (2000).

[35] T. Moriya, J. Appl. Phys. **39**, 1042 (1968).

[36] T. Yokoo, A. Zheludev, M. Nakamura, and J. Akimitsu, Phys. Rev. B **55**, 11516 (1997).

[37] J. Lorenzana and G. A. Sawatzky, Phys. Rev. B **52**, 9576 (1995).

[38] E. Gagliano, F. Lema, S. Bacci, J. J. Vicente Alvarez, and J. Lorenzana, Phys. Rev. B **62**, 1218 (2000).